Talanta 121 (2014) 163–177

Contents lists available at ScienceDirect

Talanta

journal homepage: www.elsevier.com/locate/talanta

Review

Microfluidic fabrication of multifunctional particles and their analytical applications

Xiao-Ting Sun, Mei Liu, Zhang-Run Xu *

Research Center for Analytical Sciences, Northeastern University, Shenyang 110819, PR China

ARTICLE INFO

Article history:
Received 26 November 2013
Received in revised form
20 December 2013
Accepted 25 December 2013
Available online 7 January 2014

Keywords:
Multifunctional particle
Janus particle
Microfluidic fabrication
Analytical application

ABSTRACT

Multifunctional particles have attracted extensive interest in scientific community in recent years for their capability in combining different functions within a single device. The present review focuses on the preparation methods of multifunctional particles using microfluidic techniques, and the applications of multifunctional particles in analytical and bio-analytical chemistry. As confirmed by most research works, microfluidic fabrication platforms can provide multifunctional particles with precisely controlled structure, high homogeneity and good reproducibility. Meanwhttp://live.elsevierproofcentral.com/authorproofs/macm84f82089f9eab0d214807a46cda8088e/supplier hile, multifunctional particles are proved to have enormous promise when applied in bio/chemical analysis. This paper aims to offer a path for the readers to get acquainted with state-of-the-art progress in these advanced materials from the viewpoint of microfluidics.

Contents

1. Introduction

Multifunctional particles (MPs) have drawn considerable attention of researchers in recent years. Owing to the unique feature of

* Corresponding author. Tel.: +86 24 83688944; fax: +86 24 83676698.
E-mail address: xuzr@mail.neu.edu.cn (Z.-R. Xu).

0039-9140/$ - see front matter © 2014 Elsevier B.V. All rights reserved.
http://dx.doi.org/10.1016/j.talanta.2013.12.060

bearing various functions in an integral whole, MPs have more extensive applications than monofunctional particles. As proved by a growing body of researches, MPs perform excellently in catalysis, sensing, biomedicine and display, *etc.* [1–4]. Particles possessing multiple components and properties are what is studied within the scope of MPs, mainly including anisotropic particles among which Janus particles are the most widely investigated, core–shell particles in which the core and the shell act distinct roles, as well as homogeneous particles incorporated or conjugated with other functional species. Notably, structures and functions of MPs can be flexibly adjusted to fulfill the requirements of particular applications, thus MPs are expected to open exciting opportunities in the applied fields where cooperative effect is highly desired.

Bulk production processes of MPs often come across such problems as polydispersity, poor reproducibility and lack of precision in constructing sophisticated structures [4]. The emergence of microfluidic techniques has paved a new way for fabrication of high-quality MPs. High mass and heat transfer rates, accurate control of reaction conditions, fast mixing and low reagent consumption can be achieved in microfluidic platforms [4,5], and these features make microfluidics a powerful tool in preparation of functional particles. Synthesis of MPs in a microfluidic system is greatly beneficial to controllable size and structure, high homogeneity and reproducibility, as well as simplified fabricating processes, *etc.* To the best of our knowledge, there are two major strategies in microfluidic fabrication of MPs: droplet-based method and flow-lithography-based method. The former is competent for producing spherical or sphere-like particles, while the latter is an ideal alternative for designing non-spherical particles, such as rods and flakes, which are more desirable in some particular applications. In short, microfluidics can provide a rather flexible platform for fabrication of MPs.

MPs can be designed to possess optical, electrical, magnetic or other properties that can be utilized for sensing and detecting. In fact, MPs have already shown promise in many analytical approaches. They can act as carriers in high-throughput screening, sensors for sensitive and selective detection, valves to control the fluids in lab-on-a-chip systems, as well as reporters for living cell imaging. The MPs always lead to better outcomes in comparison with monofunctional particles in these applications. The above mentioned are quite far from the entire potential applications of MPs, which could be extended to nearly every branches of analytical chemistry as the MPs can be versatilely designed.

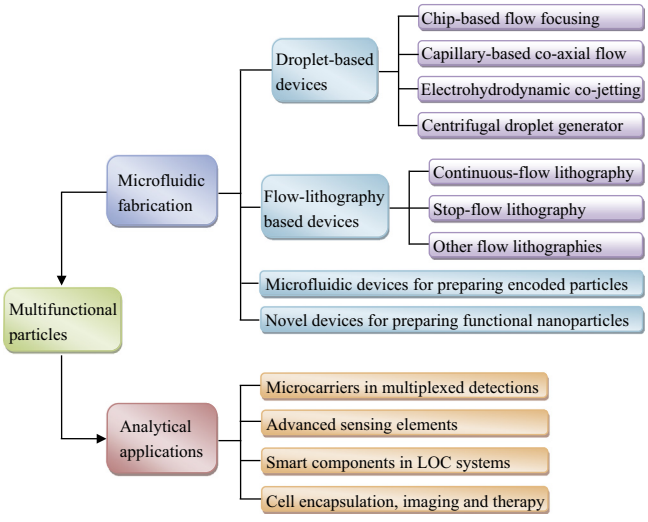

Fig. 1. Schematic diagram of the classification of microfluidic fabrication protocols and the analytical applications of multifunctional particles.

An increasing number of researches are devoted to the preparation and applications of MPs, and also there are some reviews that have summarized these studies from different points of view [1,3,4,6,7]. In this review, we will focus on the microfluidic methods for preparation and applications of MPs both in microscale and nanoscale. Fig. 1 illustrates the general organization of this article. The microfluidic fabrication methods are classified and described in detail, and representative and outstanding work is included while fresh achievements are highlighted. The present review aims to unfold the superiorities of microfluidic methods for MPs preparation and the huge potential that MPs have exhibited in analytical chemistry, which may help the readers to get acquainted with these advanced materials. Meanwhile, possible challenges are also proposed.

2. Microfluidic fabrication devices

2.1. Droplet-based devices

Microfluidic droplets are excellent templates in creating MPs, and several polymerization approaches such as UV exposition, thermal treatment, and ion-induced cross-linking are usually employed to solidify the droplets to obtain MPs. In microfluidic systems, droplets are usually formed by shear force between two immiscible fluids, which are described as dispersed phase (droplets) and continuous phase. So far, the most efficient droplet-based devices for fabricating MPs are chip-based flow focusing device (usually a main channel with two side channels on a chip) and capillary-based co-axial flow focusing device (coaxially aligned microcapillaries). Beyond these methods, other droplet-based strategies with good performances in fabricating MPs, such as electrohydrodynamic co-jetting methods and centrifuge-based droplet formation methods, are summarized as well.

2.1.1. Chip-based flow focusing

Y-shaped channel patterns are typical schemes for generating Janus particles in chip-based flow focusing methods [8,9]. As depicted in Fig. 2A, black and white monomers (carbon black and titanium oxide dispersed into an acrylic monomer respectively) were respectively introduced into the arm channels of the Y junction, and they formed stable biphasic laminar flow in the main channel. The biphasic flow was further sheared into Janus droplets by symmetrically flowing aqueous streams at the orifice. Subsequent off-chip thermal polymerization of these template droplets gave rise to bicolored Janus particles with electrical anisotropy which could be used in color switching display actuated by an electric field [8]. Flow-focusing devices combined with in situ UV-irradiation polymerization could be very efficient for the creation of Janus particles or even ternary particles (tricompartment particles) with sharp interfaces (Fig. 2B) [10]. Immiscible organic monomers M1 and M2 respectively premixed with photoinitiator were supplied to central channels either side by side (to create Janus morph) or with one inserting to the other like a sandwich (to create ternary morph), and then the monomers formed multi-phasic droplets with the help of shear force imposed by the aqueous phase W in the sheath-flow configuration. Thereafter, the droplets were polymerized into particles through UV-irradiation downstream. The fraction of M1 or M2 in a particle could be readily changed by adjusting the flow rate of each monomer.

Janus particles will play a significant role in biomedical applications for their potential synergistic actions in multiplexing, multi-level targeting and combination therapies [4]. However, UV irradiation or thermal treatment usually involved in the flow-focusing-based synthesis may cause harm to the bioactive

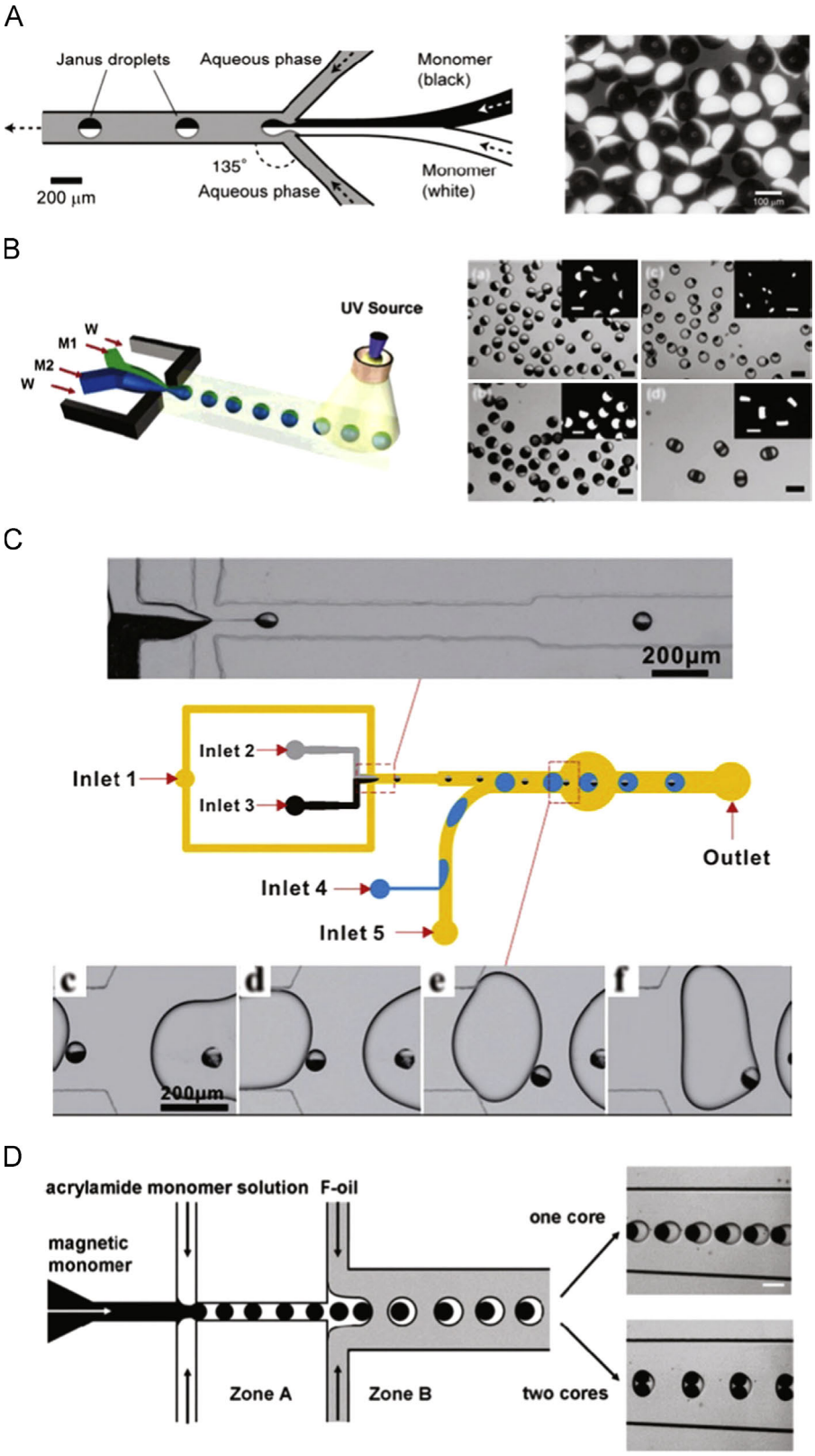

Fig. 2. Schemes of various chip-based flow focusing devices. (A) Scheme of channel and flow configuration for generating bicolored Janus particles with electrical anisotropy and the resulted particles (reproduced with permission from Ref. [8]). (B) Scheme of Janus droplet generation and Janus particles with various phase ratios and ternary particles (reproduced with permission from Ref. [10]). (C) Schematic diagram of the device used for the synthesis of magnetic Janus particles, the magnified photographs representing droplet formation and gelation process (reproduced with permission from Ref. [11]). (D) Scheme of the microfluidic device for forming double emulsion droplets (reproduced with permission from Ref. [12]). Scale bar is 100 μm in (B) and 50 μm in (D).

compounds encapsulated in the particles. Flow-focusing with a combination of droplet fusion has facilitated ion-induced cross-linking of the particles. Using this method, Janus particles composed of biocompatible alginate hydrogel were fabricated with cross-linking induced by calcium ions [11]. As shown in Fig. 2C, biphasic droplets of sodium alginate solutions with and without magnetic beads formed

at the crossing of the flow focusing configuration, and they fused with the droplets containing $CaCl_2$ to gelate in the downstream, thus Janus particles formed. The biological compatibility and UV-free gelation process of alginate hydrogel allowed for encapsulation of viable cells in the nonmagnetic hemispheres while the other hemispheres possessed a magnetic control property.

Double emulsion droplets were formed in microfluidic devices with double flow-focusing geometries, which were used to template core–shell particles by Weitz's group [12,13]. As illustrated in Fig. 2D, oil-dispersed magnetic monomer was encapsulated by aqueous solution of monomer at the first drop maker, forming oil–water single emulsion in zone A (channel walls were made hydrophilic). When flowed into the second drop maker, the emulsion was then encapsulated by oil, forming oil–water–oil double emulsion droplets in zone B (channel walls were made hydrophobic). By modulating the inner flow rate, particles with a single core (regarded as anisotropic particles) or with double cores were conveniently obtained within the same device [12].

2.1.2. Capillary-based co-axial flow

Drop formation at a capillary tip in a co-flowing continuous phase was first proposed by Cramer et al. [14]. The device of capillary-based co-axial flow can be modified for the generation of various microparticles. The device is generally of co-flow geometry or flow-focusing geometry, both of which are composed of a series of coaxially assembled microcapillaries [15]. In the co-flow device, the dispersed phase flows inside the inner capillary while the continuous phase flows in the outer capillary. Flow directions of both phases are the same, and drops form at the orifice of the inner capillary. In the flow-focusing device, both phases flow in the outer capillary but in opposite directions, and the dispersed phase is focused into the inner capillary by the continuous phase. The co-axial flow device is applicable to synthesizing MPs with regular spherical appearance, in that this device yields shear force around the inner fluid rather than lateral shear in chip-based flow focusing. Electroresponsive Janus balls with structural colors were obtained from an optofluidic system based on a co-flow geometry [16]. A pair of inner capillaries was used to make biphasic droplets. Two different suspensions were prepared for the production of highly monodisperse emulsion drops. One suspension was composed of pure silica particles dispersed in ethoxylated trimethylolpropane triacrylate resin (ETPTA). Silica nanoparticles would spontaneously assemble into face-centered cubic (fcc) structures in highly viscous resin, which could exhibit structure colors induced by the fcc lattice. Another suspension was composed of silica and carbon black particles dispersed in ETPTA, which would induce electrical anisotropy. Both suspensions were pumped into the paired inner capillaries and further extruded into droplets by an aqueous stream flowing in an outer capillary, and then Janus balls were formed downstream by means of UV curing (Fig. 3A). Structural colors of the balls could be altered by tuning the size or the concentration of the silica nanoparticles encapsulated in the balls. It is noteworthy that the structural colors allow a wider angle of view due to their isotropic optical properties, which makes the Janus balls useful in display techniques. Proof-of-concept investigations have already demonstrated the power of Janus particles in smart bead display with anisotropic colloidal photonic crystal particles [17] and magnetic-fluorescent Janus balls [18] fabricated in microfluidic devices.

Anisotropic MPs are generally composed of distinct chemical compositions, which are difficult to fabricate even in microfluidic sytems. The multiphasic laminar flows or droplets including different compositions must be shielded from any perturbations or convective cross-mixing [19]. Spontaneous separation of species in a droplet may lead to asymmetric structures. Weitz's group investigated the fabrication of Janus particles by means of thermally induced phase separation [19] and selective adsorption of colloids [20] in droplets in capillary-based co-axial flow focusing devices. Aqueous droplets containing the mixture of polyacrylamide (PAAm, served as the hydrogel) and poly(*N*-isopropylacrylamide) microgels (PNIPAm, served as the nanoparticles) were proved to be competent in forming self-segmented morphology. When the droplets were heated at about 65 °C, thermosensitive PNIPAm became hydrophobic and congregated to one side of the droplets; while the acrylamide containing water was pushed to the other side, thus producing phase-separated Janus droplets. After exposing the droplets to UV light, Janus particles with a PNIPAm microgel-rich side and an PAAm-rich side were generated (Fig. 3B) [19]. Amphiphilic crescent-moon shaped microparticles were formed by selective adsorption of colloids in a flow focusing device based on a theta-shaped capillary. Fig. 3C shows the formation process of the Janus particles. Fluorocarbon and photocurable ETPTA were respectively injected into the compartments of the theta-shaped capillary, and ETPTA phase partially wetted the oil drop at the tip of the capillary. When the droplet was released to aqueous environment, bare hydrophilic silica colloids in ETPTA spontaneously migrated and adsorbed to the interface of the droplet and water. Under UV irradiation, ETPTA was solidified to form crescent-moon-like Janus particle with a hydrophilic convex surface and a hydrophobic concave surface after the non-polymerizable fluorocarbon was removed. The amphiphilic microparticles can be used to stabilize oil droplets in water [20].

A combination of co-flow geometry and flow-focusing geometry enables controlled fabrication of multiple emulsions [15], which can act as templates for multifunctional core–shell particles with quantum dot (QD) barcodes and magnetic anisotropy [21] or tunable shell structures [22]. Anisotropic magnetic barcode particles with two separate cores or with a Janus core were fabricated by using double-emulsion droplets with two inner droplets of distinct phases as templates (Fig. 3D). For the microfluidic devices for generating double-emulsion droplets with multiple inner phases, a round capillary with two separate channels coaxially was aligned inside a square capillary. The two inner phases consisting of QD- and magnetic nanoparticle-dispersed ETPTA fluids were injected into the separate channels. And in the same direction, the middle aqueous phase flows through the region between the inner round capillary and the outer square capillary. To avoid fusion of the two types of inner droplets, surfactants were added in the middle aqueous phase which would further serve as the shells of particles. The outer oil phase flows, in the opposite direction, through the region between the round collection capillary and the outer square capillary, and hydrodynamically focuses the middle phase containing the innermost droplets, and the resultant jet breaks up into monodisperse oil/water/oil double-emulsion drops. By switching the flow on and off sequentially, double-emulsion templates with desired structures could be flexibly generated [21].

2.1.3. Electrohydrodynamic co-jetting

Electrohydrodynamic co-jetting devices were proposed and confirmed to be robust for producing MPs with sub-micrometer dimension by Lahann's group [23–25]. This method is based on simultaneous electrohydrodynamic jetting of polymer solutions driven by an electrical field, and it is versatile for generating MPs with diverse architectures. Taking the fabrication of Janus particles for example, different jetting solutions were respectively pumped into side-by-side aligned capillaries, and a single liquid thread was formed at the interface of the two jetting solutions when an electrical field was applied between the capillaries and the collecting substrate (an aluminium foil). And then the jetting

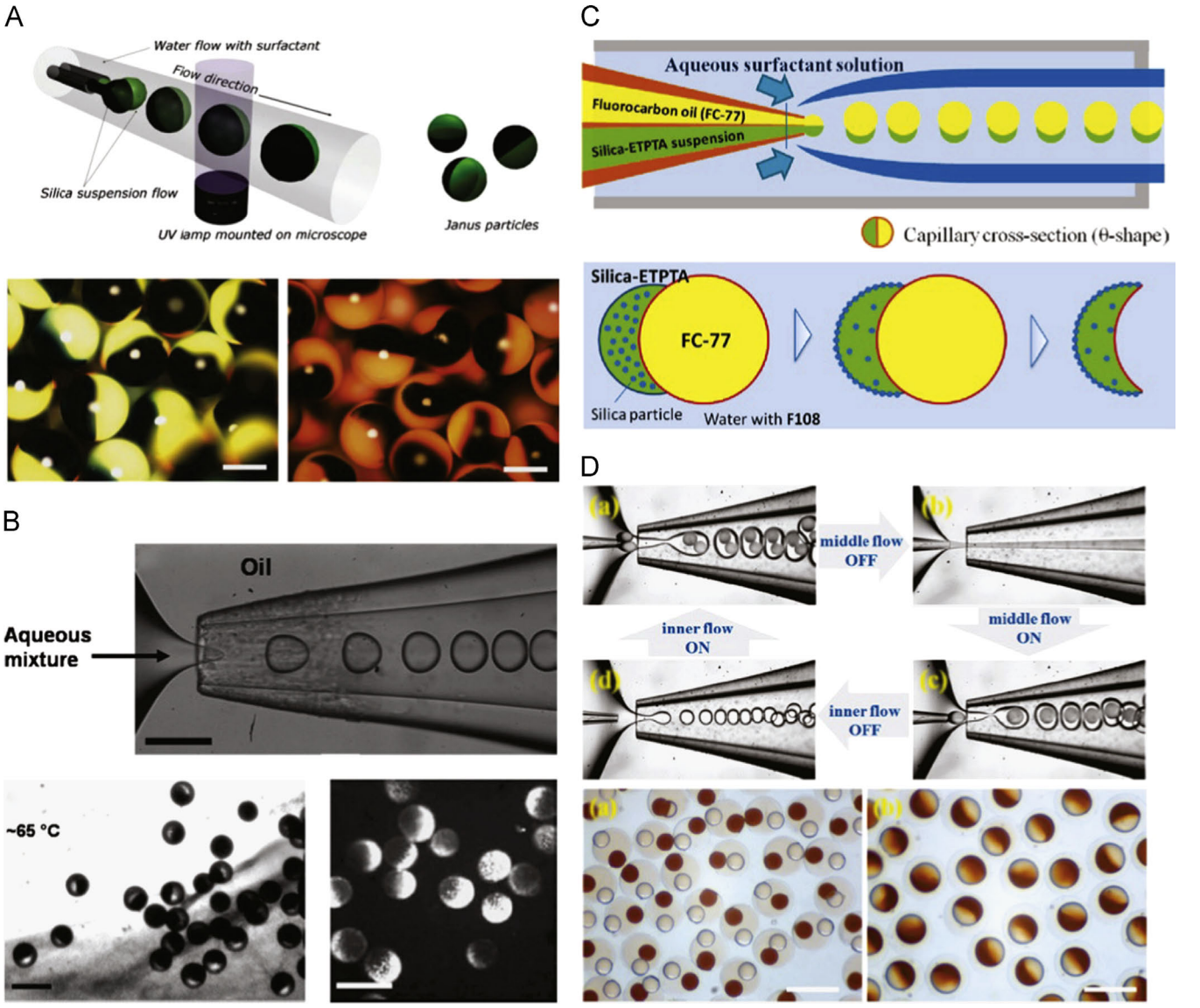

Fig. 3. Schemes and graphs of various capillary-based co-axial flow devices. (A) Scheme of optofluidic synthesis of photonic Janus balls with optical and electrical anisotropy; optical microscope images of photonic balls with different structural colors respectively comprised of 182 nm (lower left) and 198 nm (lower right) silica particles in diameter (reproduced with permission from Ref. [16]). (B) Formation of monodisperse droplets in a microfluidic device with a flow focusing geometry. The lower left image represents the phase separated droplets upon heating at about 65 °C, and the lower right image is a fluorescent microscope image of the Janus particles formed by photopolymerizing the monomers in the phase separated droplets (reproduced with permission from Ref. [19]). (C) Schematic illustration of the microfluidic device containing the theta-shaped capillary and the method to make an amphiphilic microparticle from a paired droplet (reproduced with permission from Ref. [20]). (D) Formation of double emulsions with two distinct inner phases in a glass microcapillary device, and bright-field microscope images of the polymerized double emulsions with two separate cores (lower left) and single Janus cores (lower right). The light part is the QD-tagged core, and the brown part is the magnetic nanoparticle-tagged core (reproduced with permission from Ref. [21]). Scale bars are 200 μm in all the images.

liquids were fragmented into droplets that could be collected on the substrate (Fig. 4A) [23]. Anisotropic particles with sub-micrometre diameters are accessible through electrohydrodynamic co-jetting and may be broadly applicable as nanocolloids in the fields of drug delivery, molecular imaging, and smart displays. This method was afterward extended to create more complex triphasic particles by using three distinct jetting solutions in a similar device (Fig. 4B) [24]. By changing the relative conductivity of two jetting solutions, the higher conductivity solution would be encapsulated by the lower conductivity one when the solutions jetted into droplets under an electric field, giving rise to well-defined core–shell particles (Fig. 4C) [25]. Taking advantage of the flexibility of the jetting process, microfibers with narrow size distribution were devised [26], and diverse multicompartment microcylinders (Fig. 4D) were also manufactured using electrohydrodynamic co-spinning and an automated microsectioning device [27]. In general, electrohydrodynamic co-jetting strategy is a powerful tool for the synthesis of multifunctional materials with controllable microarchitecture and sub-micrometer scale. Improving homogeneity of the Janus or multiphasic nanoparticles fabricated using this method will make these particles more powerful in bio-applications.

2.1.4. *Centrifuge-based droplet generator*

Centrifugal microfluidics exhibits huge potential not only in manipulation of microfluids but also in creation of MPs with complex structures [28,29]. Particles with two to six distinct compartments were synthesized using centrifugally rotating

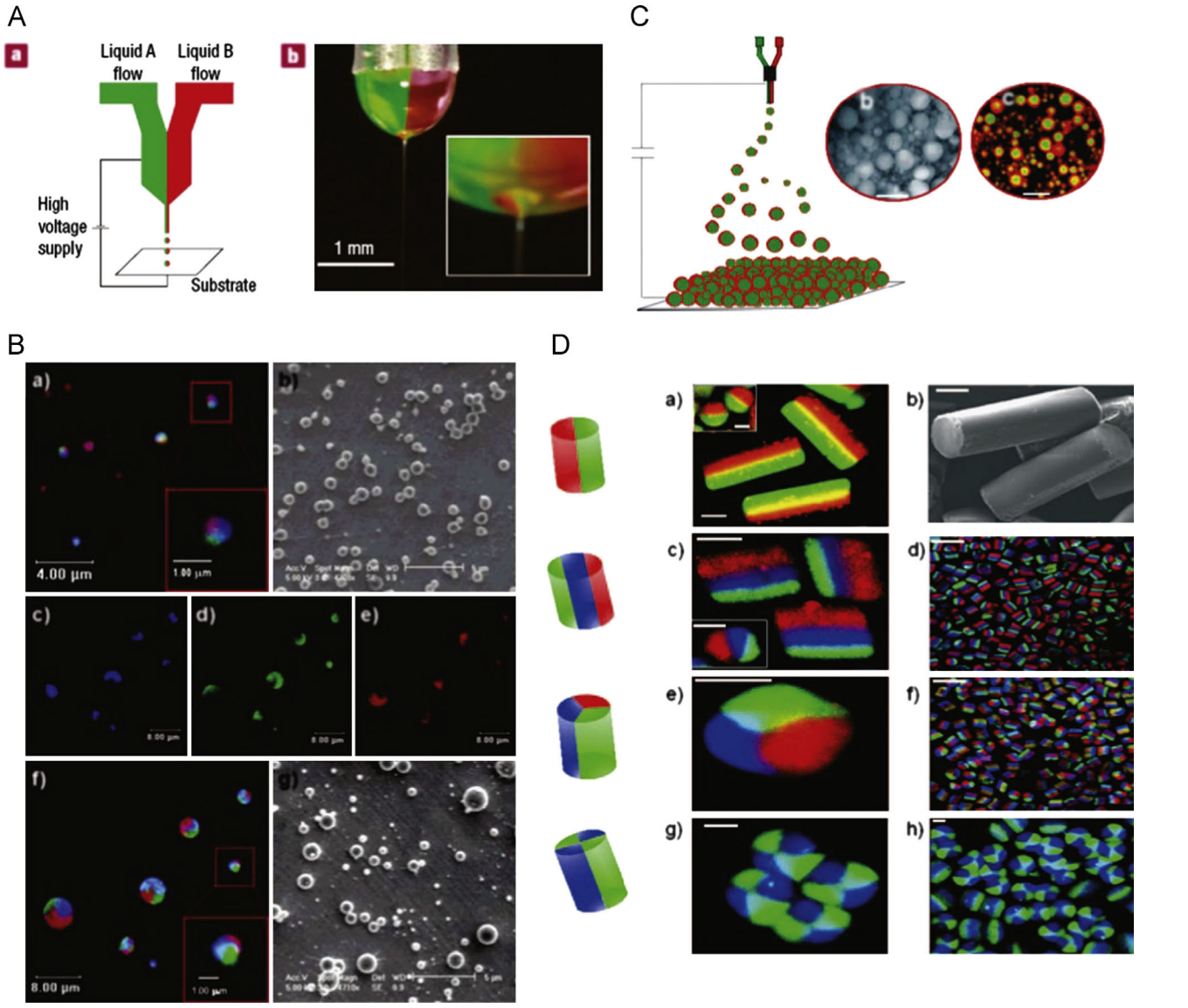

Fig. 4. Schemes of electrohydrodynamic co-jetting devices and micrographs of typical particles. (A) Biphasic electrified jetting using side-by-side dual capillaries. (reproduced with permission from Ref. [23]). (B) First row: Confocal laser scanning microscopy images and scanning electron microscopy images of poly(ethylene oxide) triphasic particles; second and third rows: colloidal particles made of poly(acrylamide-*co*-acrylic acid) and poly(acrylic acid) (reproduced with permission from Ref. [24]). (C) Schematic illustration of the electrified-jetting setup and microscopy images of the core–shell microspheres after jetting (reproduced with permission from Ref. [25]). (D) Microscopy images of multicompartment microcylinders (reproduced with permission from Ref. [27]). Scale bars are 8 μm in (C), 10 μm in (D) except for the second and third images (50 μm) of the right column in (D).

multi-barreled capillaries. Fig. 5A depicts the synthesizing process of double-compartment particles [28]. Sodium alginate solutions with different fluorescent dyes were separately introduced into two barrels of a capillary which was fixed by an acrylic holder in a microtube containing $CaCl_2$ solution in the bottom. While the microtube was centrifuging in a tabletop centrifuge, sodium alginate solutions in each capillary barrel were pumped out from the capillary and formed into Janus droplets when the centrifugal gravity was strong enough. Then the droplets traveled into $CaCl_2$ solution and were quickly gelified to particles. Using multi-barreled capillaries, even six-compartment particles were successfully procured (Fig. 5B). During the synthesis process, clear interfaces of the particles were achieved attributing to the immediate formation and gelation of the droplets. However, the difficulty in interfacing the rotating microdevice and external instruments has prevented this method from achieving continuous and higher throughput production.

2.2. Flow-lithography based devices

One limitation of droplet-based devices is that most of the produced particles are restricted to spherical or sphere-like appearance since their morphs strictly depend on the template drops. However, particles with complex structures are more desirable in some cases. Microscope projection photolithography techniques for fabricating MPs with various shapes in microfluidics have been introduced and deeply researched by Doyle's group [30–32]. Flow-lithography designs mainly involve co-flowing laminar streams of photo-curable chemicals in microfluidic channels and a focused UV light beam shaded by a transparency mask, through which the shape and size of the particles are controlled. This flexible photolithography technique offered a distinct advantage in designing non-spherical particles with diverse functions, like cuboid [30], wedge [33], barcode [34], or even more complex structures [35–37].

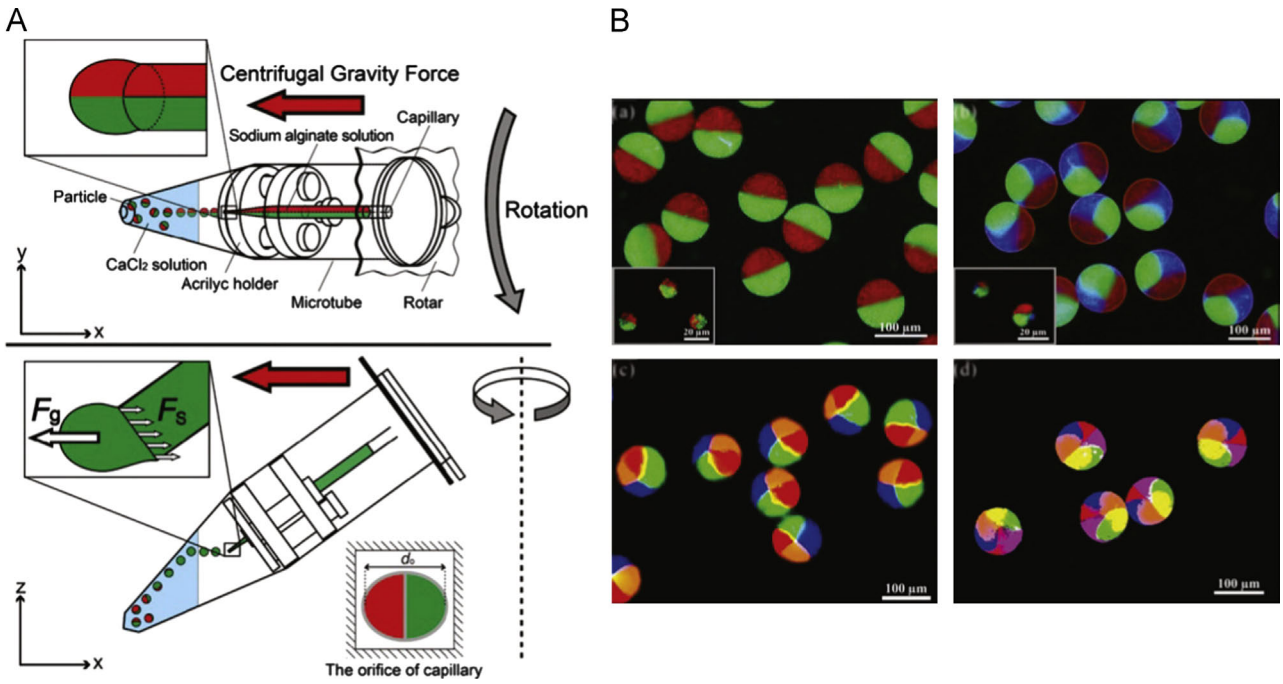

Fig. 5. (A) Centrifuge-based droplet formation from multi-barreled capillaries. (B) Particles possessing multi-compartment body compositions with axisymmetrical geometries. Insets show the satellite particles (reproduced with permission from Ref. [28]).

2.2.1. Continuous-flow lithography

Cuboid particles with fluorescent asymmetry were synthesized in a continuous-flow lithography (CFL) system (Fig. 6A) [30]. A transparency mask with desired features was inserted into the field-stop of an inverted microscope to confine the UV light beam. When rhodamine-labelled acrylate oligomer and fluorchrome-free oligomer were co-flowing in a polydimethylsiloxane (PDMS) channel, bifunctional Janus particles were synthesized by polymerizing rectangular particles across the interface of the co-flowing streams using the mask-defined UV light beam. The particles were subsequently flushed out by the unpolymerized oligomer stream rather than stuck to the channel surfaces attributing to the phenomenon of oxygen inhibition at the PDMS walls. The ratio of different chemicals within a particle could be adjusted by controlling the location of the co-flow interface and the UV beam. Later, more functional encoded particles [31] and wedge-shaped amphiphilic particles [33] were synthesized using CFL. Compared with traditional lithography techniques, the continuous-flow lithography strategy allows for higher throughput (400,000 particles h^{-1}) generation of polymeric particles. However, high throughput and high resolution can not be achieved simultaneously because particles are synthesized in continuous flow and exposed to finite pulses of UV light.

2.2.2. Stop-flow lithography

On the basis of CFL, stop-flow lithography (SFL) was proposed by Doyle's group [38], which provides a preferable way for the synthesis of complex particles at the colloidal length scale with improved resolution, sharp interfaces and high throughput. Compressed-air driving method was selected to switch between stop and flow mode in SFL, and flowing streams of oligomers can be immediately stopped to undergo the UV-induced polymerization and restarted flowing at a high flow rate (Fig. 6B). Unlike CFL in which the particles are smeared at high oligomer flow rates, SFL can produce high resolution particles ascribing to the "stop-polymerize-flow" process, and this cyclic process with a high flow rate permits remarkable improvement in synthesis throughput. This technique afforded the ability to create poly(ethylene glycol) (PEG)-based encoded microparticles with spatially discrete regions [34]. The PEG-based microparticles consisted of the encoded, control, and capture DNA regions, which were copolymerized seamlessly by a single UV exposure through a photomask with the desired microparticle shape. As confirmed by the experimental results, tobacco mosaic virus nanotemplates could hierarchically assemble onto the microparticles with high spatial and sequence selectivity via nucleic acid hybridization. SFL is a very flexible strategy to yield newfangled MPs, such as microparticles with tailored degradation behavior [39] or with controlled encapsulation and release functions [40] which are promising candidates for drug therapies.

2.2.3. Other flow lithographies

Sophisticated particles with various spatial morphologies may present greater potentials for a host of applications in biomedicine and engineering. On the basis of flow lithography, derivative devices were developed to meet the desire for fabricating particles with 3D configuration. A stop-flow interference lithography (SFIL) technique that integrated the complementary aspects of phase-mask interference lithography (PMIL) with SFL enabled the high-throughput synthesis of three-dimensionally patterned, transparency-mask-defined polymeric particles with sub-micrometer feature sizes (Fig. 7A) [35]. Two masks with distinct functions were employed in SFIL approach: a transparency mask to define the shape of particles, and a phase mask to induce 3D distribution of light intensity to produce 3D structure of the particles by selective cross-linking of the oligomer. It was shown in this work that the high ratio of surface area to volume of the structures, which originated from the intricate patterned networks of the particles, may be used to generate high fluorescent signal intensities that could be of benefit to a variety of sensing and diagnostic applications.

Lock release lithography (LRL) [36] and hydrodynamic focusing lithography (HFL) [37] were subsequently established to allow for the production of 3D particles with more complex morphologies.

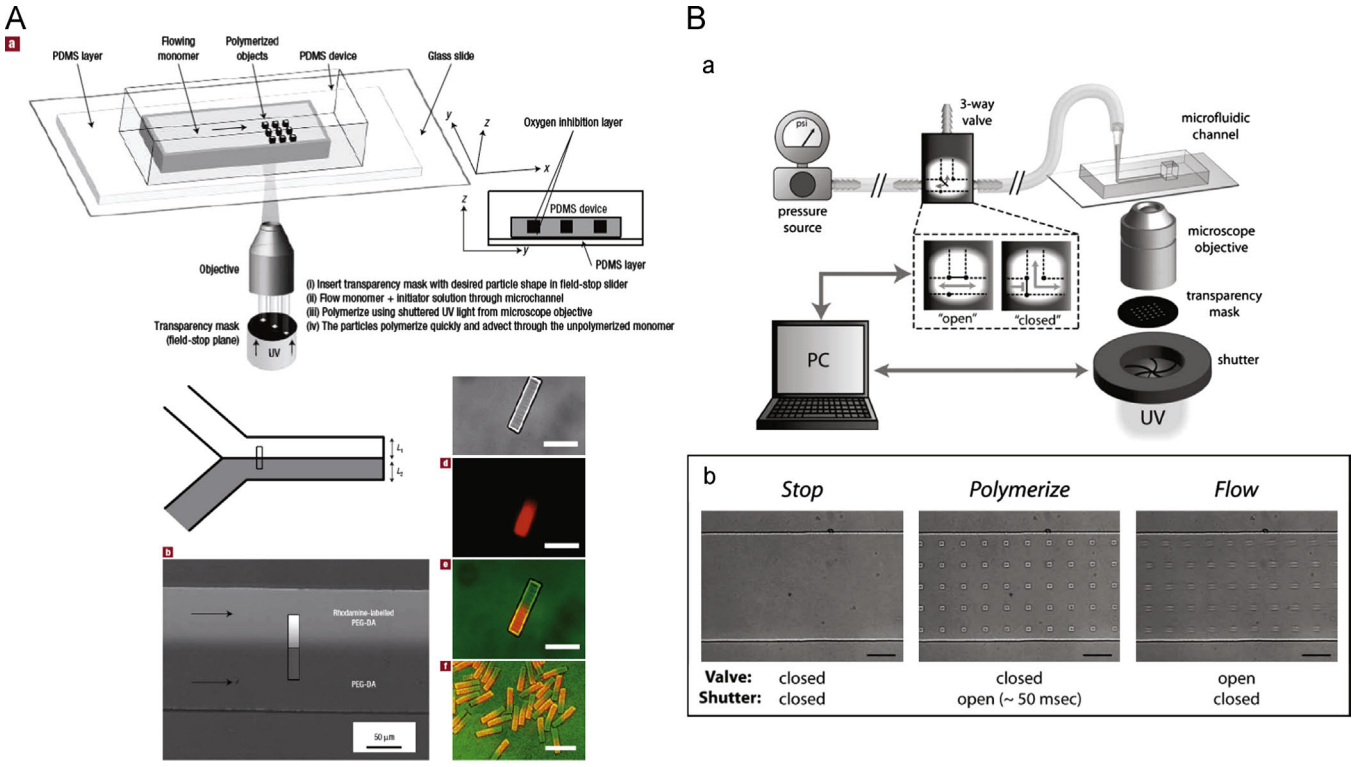

Fig. 6. (A) Schemes of continuous-flow lithography device and microfluidic geometry for fabricating cuboid Janus particles and images of the particles (reproduced with permission from Ref. [30]). (B) Scheme of stop-flow lithography device and microscope images showing the "stop-polymerize-flow" process (reproduced with permission from Ref. [38]). Scale bars are 100 μm in (A) and 50 μm in (B).

LRL utilized a combination of channel topography, mask design, and pressure-induced channel deformation to form and release particles in a cycled fashion. In the example shown in Fig. 7B, a channel with positive relief features in the topology was used to lock in an array of particles that were formed by UV exposure through a transparency mask, and particle morphology was defined by a combination of mask feature and channel topography [36]. Afterwards, a relatively high pressure was applied to PDMS channels to initiate flow and deflect the channel to release the particles. With LRL, composite particles with spatially configurable chemistries were synthesized (Fig. 7C). However, most flow-lithography (FL)-based approaches for generating particles with patterned chemistries need to align the masks precisely at the interfaces of the multiple flows, which are rather time-consuming and to some extent limit the throughput. And apparently, anisotropic features of the particles are confined to the *x*, *y* plane, whereas particles with *z* direction anisotropy can not be created using these approaches. To address these shortages, HFL was developed [37]. In this approach, the fluid interface can be perpendicular to the UV light propagation direction, and therefore precise mask alignment at the interface is no longer needed. This change in orientation of the fluid interface allows for production of 2-D arrays, which could lead to an over 200 times higher throughput compared to traditional SFL. In HFL, multiple monomer streams can be simultaneously stacked in both the *z* and *y* direction leading to more complex particles. Fig. 7D shows the synthesis process of triangular particles composed of two layers. In the stacked flows formed in two-layered channels, double-layered triangular particles were synthesized through a mask with triangles. By stacking multiple flows that sequentially entered from the bottom layer, tri-layered particles were generated (Fig. 7E upper). Especially by using a 2-D flow-focusing geometry, dual-axis particles were also successfully created (Fig. 7E lower).

2.3. Microfluidic devices for preparing encoded particles

Particle-based suspension array is believed to be a promising tool for multiplexed analysis, in which it is significant to generate encoded particles with large coding capacity and robust target binding ability. To produce such encoded particles, many microfluidic methods were exploited, and encoded particles produced in microfluidic systems mainly involve graphically and spectrally coded particles. As mentioned above, flow lithography device is an admirable tool for synthesizing graphically encoded particles which can bear over a million unique codes. Fig. 8A shows the synthesis of dot-coded particles through polymerizing across two adjacent laminar streams to make single-probe, half-fluorescent particles. The particles comprised of a fluorescent code region that contained unpolymerized dots as coding elements, as well as one or more probe regions that incorporated with bio-probes for capturing analytes [31]. To read the informations carried by each particle, these particles were aligned by using flow-focusing in a flow-through microfluidic system, and then the images of particles were taken as the particles passed the detection region (shown in Fig. 8B). The image sequences were later analyzed to determine the particle code and to quantify targets. Reflection spectra-coded colloidal crystal beads were created through a bottom-up self-assembly process using microfluidic droplets by Gu's group [41–43]. For silica colloidal crystal beads (SCCBs) fabrication, an aqueous suspension containing monodisperse silica nanoparticles was cut off into monodisperse droplets in a T-shaped microfluidic droplet generator, and the resulted droplets were collected and heated to allow for evaporation of solvent and aggregation of the nanoparticles, resulting in formation of colloidal crystal beads with silica nanoparticles self-assembled in close-packed structures (Fig. 8C). Calcination was employed to improve the mechanical stability and lower the fluorescent background of the beads. By changing the

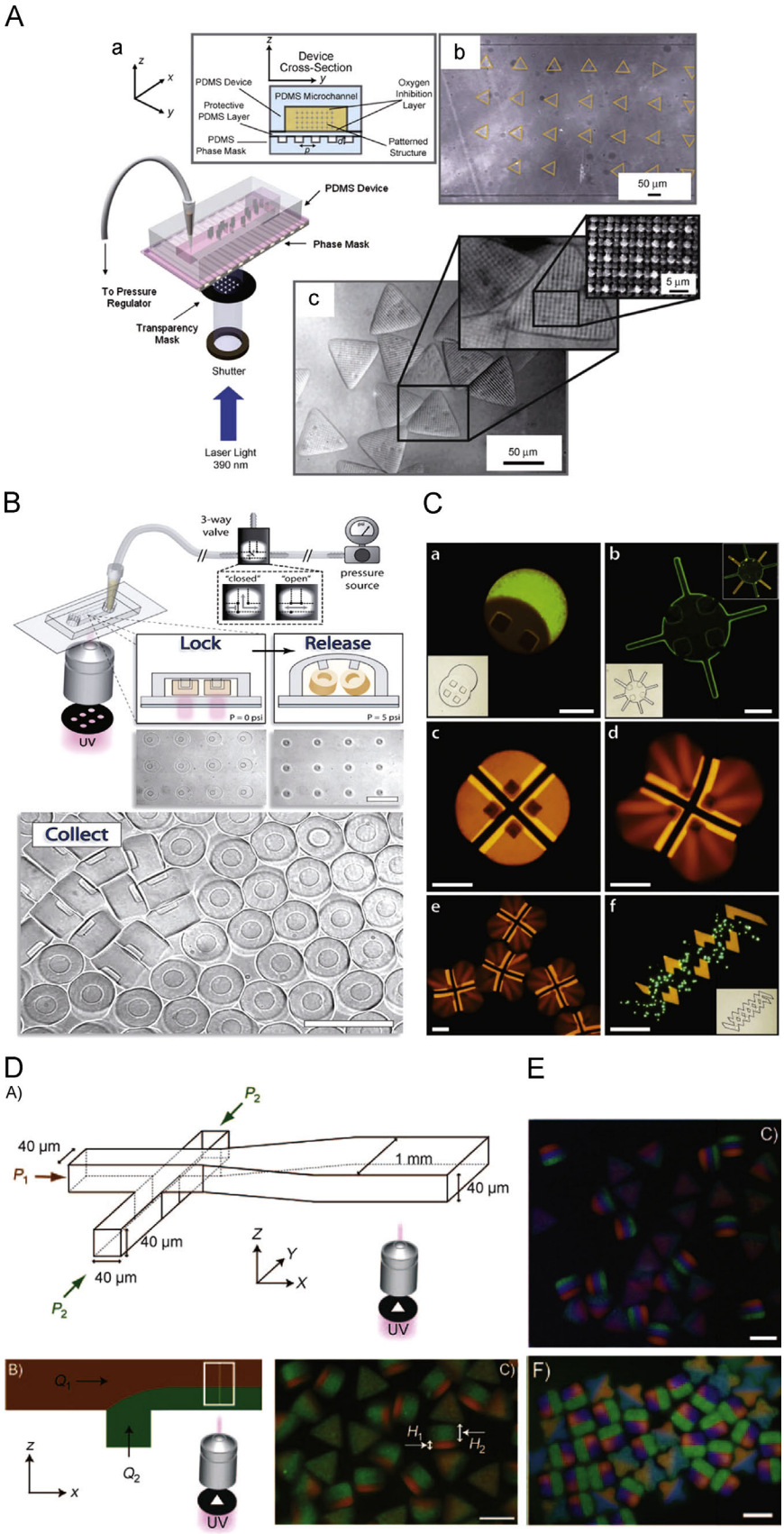

Fig. 7. (A) Schematic drawing of stop-flow interference lithography device and images of the resulted particles (reproduced with permission from Ref. [35]). (B) Scheme of lock release lithography (LRL) process and the collected 3D particles, (C) Fluorescence and differential interference contrast images (insert, outlined for clarity) of various functional particles fabricated using LRL method (reproduced with permission from Ref. [36]). (D) Upper: schematic of the microfluidic device used in HFL; lower: a side view of flow focusing and a fluorescent image of double-layered triangular particles. (E) Fluorescent images of trilayered triangular particles (upper) and cross-shaped dual-axis layered particles (lower) (reproduced with permission from Ref. [37]). Scale bars are 100 μm in (B), 50 μm for images at the first row in (C) and 100 μm for others in (C), 50 μm in (D), 50 μm for the upper image in (E) and 40 μm for the lower image in (E).

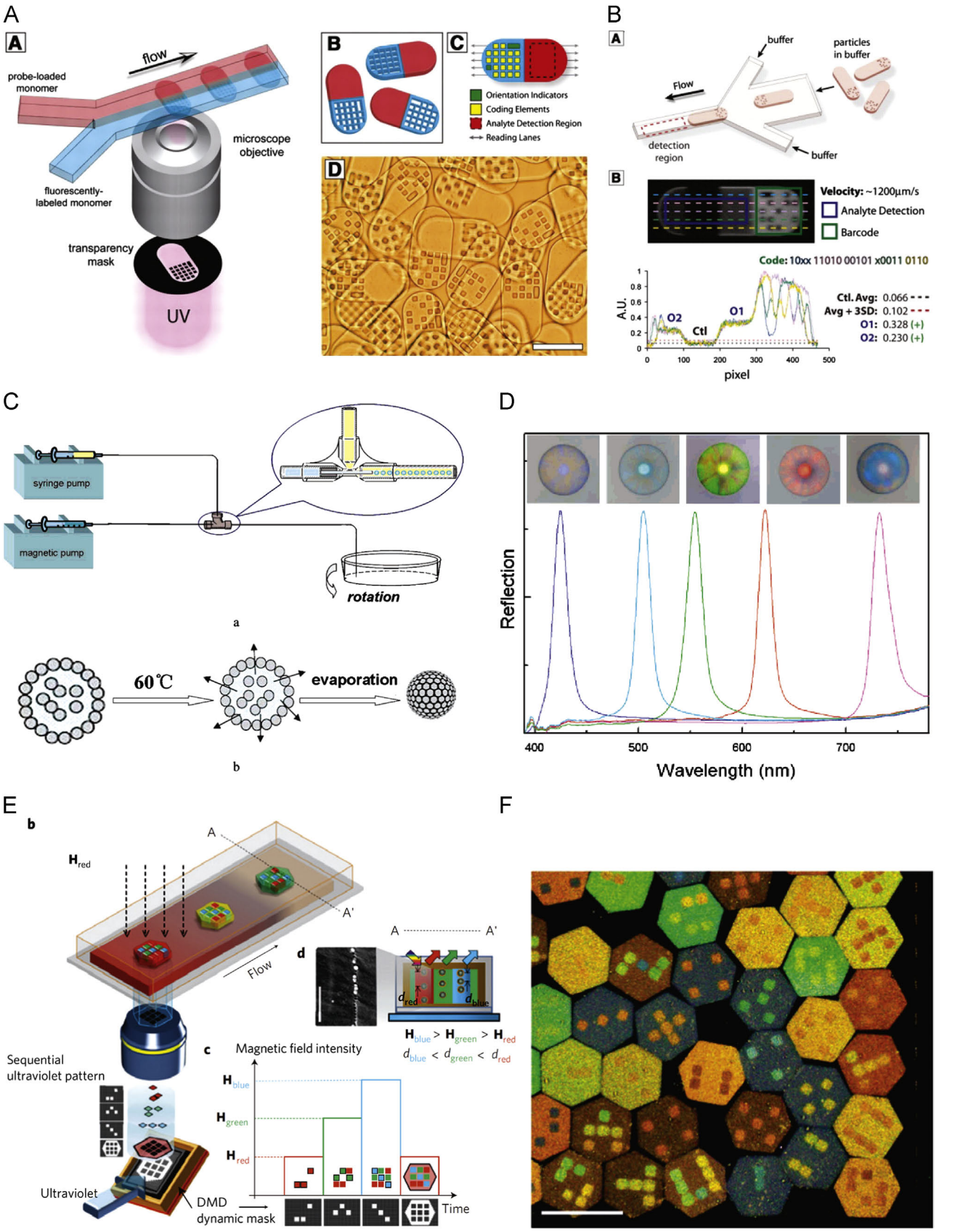

Fig. 8. Schematic diagram of various devices for fabricating encoded particles and images of encoded microparticles. (A) Scheme of dot-coded particle synthesis using FL strategy and differential interference contrast image of the particles. (B) Flow-through particle reading. Upper: the flow-focusing microfluidic device used to align and read particles; lower: scanning of fluorescent intensity across the five lanes of the multiprobe particle to reveal the code and detect the targets (reproduced with permission from Ref. [31]). (C) Illustration of the T-shaped microfluidic device and solidification process for SCCBs. (D) Reflection spectra of the beads composed of silica nanoparticles in different sizes. The sizes of the particles are 200, 225, 240, 260, and 295 nm from left to right (reproduced with permission from Ref. [43]). (E) Conceptual description of the process of generating colour-barcoded magnetic microparticles. (F) Hexagon-type 2D colour-barcoded microparticles (reproduced with permission from Ref. [44]). Scale bars are 100 μm in (A) and 500 μm in (F).

diameters of the silica nanoparticles, a series of SCCBs with different diffraction peak positions were obtained, which were further used for encoding (Fig. 8D) [43]. In contrast to commonly used spectrum-encoding elements that are based on fluorescent dyes and quantum dots, the coding method based on reflection spectra does not encounter fluorescence quenching or bleaching, bio-toxicity and spectral overlap.

The spectral coding methods are practically limited by the availability of the different indicating materials with minimal spectral overlap, and the binary graphical coding methods are limited by the particle size. To overcome the limitations, a novel color barcoding strategy based on a microfluidic platform was developed recently [44]. A single M-Ink (composed of photocurable resin monomer solution and superparamagnetic colloidal nanocrystal clusters (CNCs)) was utilized to fabricate microparticles with two-dimensional colour barcodes, and a sequential process was used involving the cooperative actions of magnetic-field modulation and spatially controlled ultraviolet exposure. M-Ink was filled in PDMS channel firstly. The colour of M-Ink can be tuned by modulating an external magnetic field which changes the periodicity of the 1D chain structures of the superparamagnetic CNCs. Once the desired colour for a specific code was set by the magnetic field, the UV mask pattern of the desired barcode was illuminated to locally fix the colour by "freezing" the 1D chain structure of the superparamagnetic CNCs in M-Ink. Making the next barcode bit using a different colour was done simply by changing the pattern and the magnetic field intensity (Fig. 8E). Producing microparticles with eight different colour codes took only about 1 s. Various types of colour barcoded microparticles were demonstrated, and Fig. 8F shows hexagon-type 2D colour-barcoded microparticles. It is worthy to mention that this color barcoding method allows for a remarkable increase in coding capacity compared to conventional binary coding. Red-green-blue levels of individual code positions were obtained from reflection micrograph and digitized for decoding.

2.4. Novel microfluidic devices for preparing functional nanoparticles

Functional nanoparticles are highly desired in biomedicine. Restricted by the dimension of fluids in microchannels or the light beams used to induce polymerization, the size of functional particles fabricated using microfluidic strategies is usually at 50–200 μm. The fabrication of MPs at nanometer scale in microfluidic systems remains a challenging work. Efforts have been devoted to address this challenge, for instance, electrohydrodynamic co-jetting strategy discussed above has already been proved to be robust for nanoparticle fabrication [23–25]. Besides, laminar flows and droplets in microchannels are also exploited for solving this problem. Farokhzad et al. [45] used rapid and tunable mixing through hydrodynamic flow focusing in microfluidic channels to control nanoprecipitation of poly(lactic-*co*-glycolic acid)-*b*-poly (ethylene glycol) (PLGA-PEG) diblock copolymers to make polymeric nanoparticles for drug delivery. The narrow width of the focused stream enabled rapid mixing through diffusion between polymer and organic solvent solution and water, which gave rise to spherical nanoparticles with PLGA core–PEG corona structure. It was demonstrated that microfluidics was efficient for nanoprecipitation synthesis of smaller and more homogeneous PLGA-PEG nanoparticles in comparison with bulk synthesis. Recently, a fluidic nanoprecipitation system has also shown promise in fabricating polymeric Janus nanoparticles [46]. Taking microfluidic droplets as micro-reactors provides unique advantages over conventional strategies in synthesis of nanoparticles [47,48]. Continuous plasmonic nanoparticle synthesis in microfluidic composite foams was presented through a seeded growth procedure [47]. Gas bubbles and aqueous drops containing reagents for nanoparticle synthesis were alternately generated, forming the composite foam lattice. The foam generation system enabled precise control of reagent dispensing and mixing, and the ordered foam structure facilitated compartmentalized nanoparticle growth. Uniformly sized unaggregated nanoparticles requiring no postsynthesis treatment were fabricated. Although these strategies have shown potential in fabrication of nanoscale MPs in microfluidic systems, monodispersity of the particles still requires improving. Therefore precise control over particle size is a key task in microfluidic synthesis. It is expected to exploit new microfluidic approaches for fabrication of nanometer-sized MPs to meet the requirements.

3. Applications in analytical chemistry

3.1. Multifunctional encoded microcarriers in multiplexed detections

Multiplex assays are highly significant in the fields of genetic and proteomic analysis, drug screening, clinical diagnosis and so on. Particle-based suspension arrays provide multiplexing strategies with high flexibility, low cost and high throughput [49]. Encoded particles with functions of coding and probing have contributed to high-throughput detection of various proteins [32,41–43,50–52] and nucleic acids [31,53–59]. In a typical experiment in which graphically encoded particles were utilized for protein detection [32], the targeting process involved assembling an antibody sandwich around the target protein by exposing particles to the sample, adding a biotinylated reporter antibody and labeling the bound reporters with a streptavidin–phycoerythrin complex. For decoding and target quantitation, a multistage-flow-focusing microfluidic device was used to make the particles precisely align in the central channel and pass through a thin exciting window in the detection zone. Fluorescence emitted from the code region and probe region of a particle was detected by a PMT to reveal the code and report the content of the targets. Compared with other particle-based assays, the coding capacity of this strategy was distinctly improved without affecting target detection performance. Additionally, a versatile microfluidic flow scanner was developed for decoding particles and quantifying the amount of bound target. By using the bar-coded hydrogel microparticle-based detection platform, high-throughput (25 particles per second) and sensitive (a detection limit of 1 pg/ml) analysis was achieved. In general, target detection in the suspension arrays is realized by detecting the labels attached to the biomolecules, while the labeling process is tedious and time-consuming, and some labeling reagents are toxic. Label-free detection performed with suspension arrays based on spectra-coded photonic beads was developed by Gu's group [52,58,60]. In the case of label-free multiplex detection of human tumor markers, inverse-opaline photonic beads with different diffraction-peak positions and colors were used as micro-carriers for the suspension array [60]. The beads were first modified with probe antibodies, and the known reflection peaks of the probe-modified beads were used for encoding. And then antigens would specifically bind to the probe antibodies, resulting in a change in the average refractive index of the beads, and this change could be detected as a corresponding shift in the diffraction-peak position. The shift in the peak position could be used to quantitatively estimate the amount of bound antigen. The method was rather sensitive, and even a trace amount of Human CA19-9 (50 U mL^{-1}) was enough to demonstrate a change of the reflection peak. By using different beads with distinct reflection-peak positions and colors as encoded carriers, label-free multiplex immunoassays were realized. Furthermore, a microfluidic flow-through device was developed for high-throughput detection of the beads. In the reflection spectrum-based multiplex analyses,

the labels, which might hinder the activity of biomolecules, are no longer needed.

3.2. Advanced sensing elements

Sensors based on MPs can provide enhanced sensitivity or selectivity over conventional sensing devices [29,61–63]. Multitargeting detection was demonstrated with multiphasic alginate microparticles that were produced in a combined needle injection system [29]. Single-phase alginate particles having polydiacetylene (PDA) liposomes were fabricated and confirmed to facilitate a 20-times better sensitivity when used as melamine detection sensors compared to conventional solution phase detection systems. Furthermore, biphasic and triphasic alginate microparticles were also developed for multitargeting detection. For triphasic particles, three different PDA liposome/alginate mixture solutions, respectively used for negative control, avidin-fluorescein isothiocyanate (FITC) sensing and melamine sensing, were co-injected into the $CaCl_2$ solution by means of the combined needle injection system. As a result, 1/3 fraction of the particles represented green fluorescence after the incubation of the particles in an avidin-FITC solution, and additional red fluorescence was developed in the adjacent 1/3 fraction after subsequent incubation in a melamine solution (Fig. 9A). The results indicated that the particles were promising in multitargeting detection and presented a great potential for the development of advanced biosensors having a high-throughput screening capability.

Highly sensitive detection was also achieved by using MPs and a surface-enhanced Raman scattering (SERS)-based microfluidic sensor [61]. Trace mercury(II) in water was detected based on aptamer-modified Au/Ag core–shell nanoparticles in microfluidic droplets. Probe DNA-embedded gold nanoparticles were encapsulated with silver to maximize the Raman signals. In the presence of mercury(II) ions, aptamer DNAs were released from nanoparticle surfaces by forming a more stable T-mercury(II)-T mediated hairpin structure, and therefore a decrease in SERS signals was observed (Fig. 9B). A pentagon-shaped microfluidic channel along with winding channels was designed to allow droplet formation

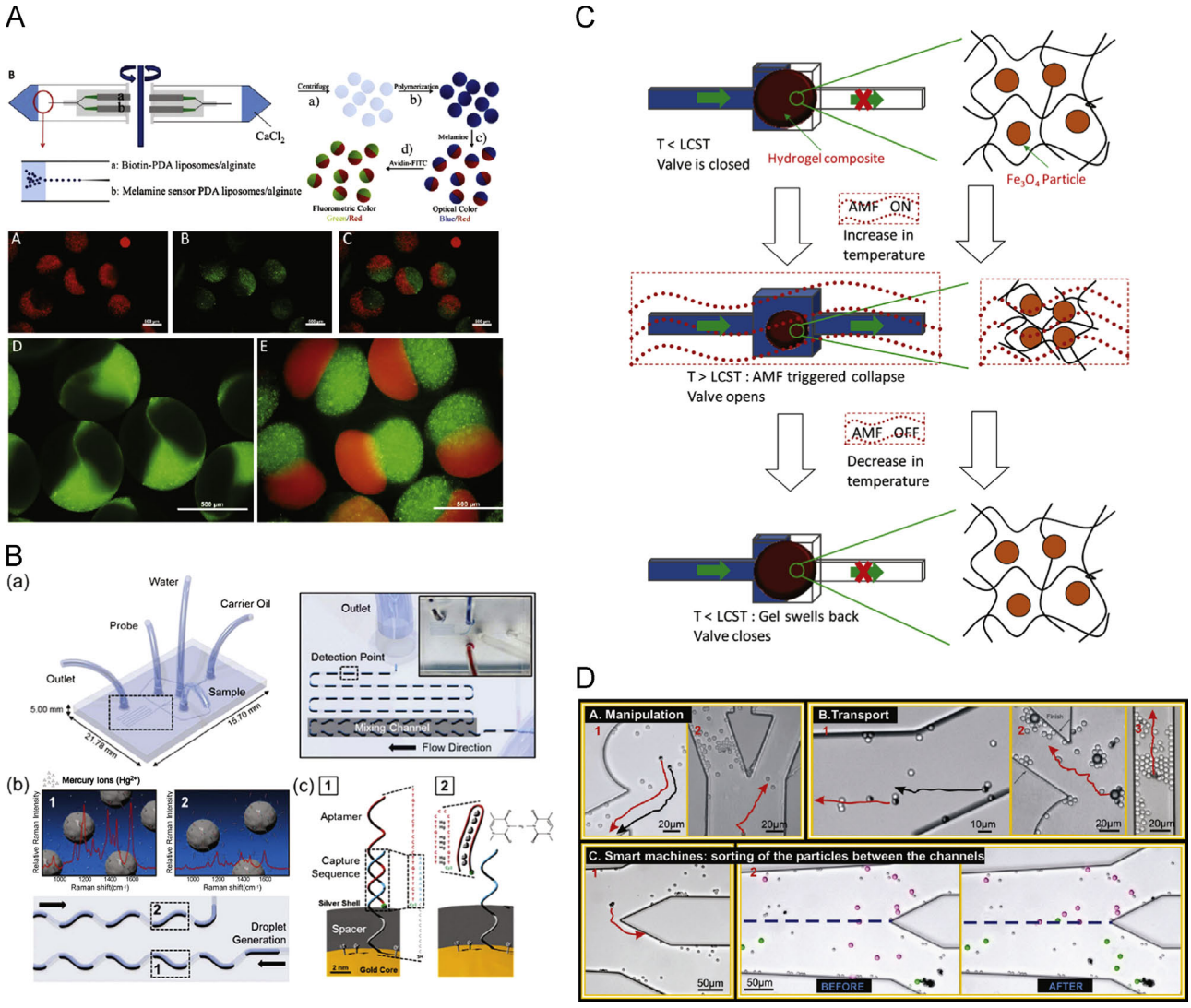

Fig. 9. Applications of MPs in sensing and lab-on-a-chip systems. (A) Scheme for the fabrication of biphasic alginate particles having embedded PDA liposomes, and fluorescence microscope images of the multiphasic alginate particles having different PDA liposomes after incubation with avidin-FITC and melamine (reproduced with permission from Ref. [29]). (B) SERS detection of mercury(II) using aptamer-modified Au/Ag core–shell nanoparticles in microfluidic droplets (reproduced with permission from Ref. [61]). (C) Schematic of the concept of remote controlled hydrogel nanocomposite valves with an alternating magnetic field (reproduced with permission from Ref. [66]). (D) Manipulation of magnetic Janus motors by applying an external magnetic field for cargo transportation and particle sorting (reproduced with permission from Ref. [67]).

and high efficiency mixing among the mercury(II) solution, buffer, and aptamer probes in each droplet. The amount of mercury(II) was evaluated by detecting the SERS signal drop, and the LOD was estimated to be below 10 pM. Additionally, the microdroplet sensor made reproducible quantitative analysis possible, and this strategy could be used as an in-the-field sensing platform due to its size and simplicity.

3.3. Smart components in lab-on-a-chip systems

Great attention has been devoted to develop new functional components for advanced manipulation of fluids and species in lab-on-a-chip systems. For example, remote controlled flow regulation or species sorting through smart components is of great value for their high flexibility. Micro-valves and switches constructed from MPs have already been developed [64–66], and particle separation, cargo transportation and sorting were realized with MPs as well [67–69]. A hydrogel nanocomposite microfluidic valve was developed for remotely controlled flow regulation [66]. Magnetic nanoparticles were dispersed in temperature-responsive *N*-isopropylacrylamide hydrogels to construct the nanocomposite valve, and an alternating magnetic field (AMF) was employed to heat the magnetic nanoparticles by Néel and Brownian relaxations and in turn heat the hydrogel matrix. As the temperature of the matrix went above the lower critical solution temperature, the hydrogel would collapse opening the channel. When the AMF was turned off, the hydrogel cooled down slowly leading to swelling and a blocked upper channel. Thus, the nanocomposite hydrogel functioned as a remotely controlled ON–OFF valve (Fig. 9C). Similarly, functional microgels composed of poly(N-isopropylacrylamide) and graphene/Fe_3O_4 hybrids were synthesized in a microfluidic reactor as switch materials [65]. The graphene materials generated heat when exposed to a near-infrared (NIR) laser, so the microgel containing graphene shrunk and swelled circularly with ON/OFF switching of NIR laser irradiation. Due to the good response of the microgel to an external magnetic field and NIR laser irradiation, a light-driven and magnetic controlled switch for fluids on a PDMS chip was realized. However, these stimuli-responsive hydrogel-based valves have a rather long response time (tens of seconds), which may be inadequate for fluid regulations in some cases. A Janus particle with a conducting hemisphere and a non-conducting hemisphere was proven to be feasible for switching and controlling the flows with a shorter response time in a microfluidic chip utilizing induced-charge electrokinetic motion of Janus particles [64]. Easy operation and fast response could be achieved with the Janus particle-based micro-valve.

In microfluidic systems, there is a strong demand for controlled motion and separation of species in microchannels because of their potential applications in molecule or cell separation, biosensing, drug and gene delivery, *etc*. As we can imagine, controlled motion of magnetic Janus particles can be realized by the application of an external magnetic field. Actually, separation of magnetic Janus particles [68] and targeted cargo delivery using catalytic Janus motors [67] were already accomplished in microfluidic channels. As depicted in Fig. 9D, manipulation of the free catalytic particles, cargo transportation and particle sorting were demonstrated under an external magnetic field [67].

3.4. Applications in cell encapsulation, imaging and therapy

MPs have shown great advantages and potential in the field of biomedicine due to their unique properties such as tunable dimension, biocompatibility and relatively low cytotoxicity. They have been widely applied in areas associated with living cell investigation and tumor suppression, including cell encapsulation [11,28], cell binding [70], cell imaging [71–73], drug and gene delivery [46,74–77]. In virtue of the biocompatibility of the alginate hydrogel, encapsulation of viable cells in alginate Janus particles was carried out in a microfluidic device [11]. Cells and magnetic beads could be separately embedded in one hydrogel particle to reduce the contact between the two, and the alginate cell capsules could be easily controlled and manipulated by external magnetic fields. The particles could be applied in cell culture array or targeted delivery based on magnetic control. A similar encapsulation approach was accomplished in a centrifuge-based microdroplet formation system [28]. Cells were successfully co-encapsulated with the magnetic nanobeads in Janus particles, and the viability of the encapsulated cells was 91%. Fig. 10A shows that the magnetic Janus particles carrying living cells self-assembled into pearl-chain structures under an external magnetic field.

MPs are often specifically bound to certain cells through antibody–antigen binding or streptavidin–biotin interaction for targeting, and they are employed for further imaging or therapy of the cells. To achieve spatially-controlled affinity towards human endothelial cells, bicompartmental particles were synthesized, and they were selectively modified to create anisotropic particles with two biologically distinguishable hemispheres: one exhibiting high binding affinity for human endothelial cells and the other being essentially resistant towards cell binding [70]. Increased cellular binding was observed with streptavidin-modified particles as compared to particles that were not modified. Cell imaging and tracking not only depend on specific binding, but also require that functionalized particles can be permeated or delivered into the cells. QDs coated with a poly imidazole ligand as fluorescent sensors were delivered into the cell cytosol using a novel microfluidic device [71]. In this device, cells were rapidly deformed as they passed through a constriction in a microfluidic channel, thus resulting in the formation of transient membrane disruptions, and QDs might then diffuse into the cytosol during the lifetime of these disruptions. Confocal microscopy images show that cells had diffuse cytoplasmic QD staining throughout different *z*-sections of the cell (Fig. 10B). In a more recent work, a similar microfluidic approach has demonstrated the ability to deliver a range of materials to 11 cell types [77]. Combination of imaging and siRNA delivery functions was realized using multicompartmental polymer nanoparticles [74]. The nanoparticles were produced *via* an electrohydrodynamic co-jetting process. The PLGA compartment was employed as an imaging modality, and the polyethyleneimine (PEI) compartment as an endosome sensing and escape compartment that also served as a siRNA release compartment. The imaging compartment was labeled with a blue fluorescent polymer dye, and the hydrogel compartment contained the siRNA-payload along with a transient red fluorescent dye. When the particles entered the endosome where pH values were generally lower than 7.4, the pH-sensitive PEI compartment allowed sensing of the endosomal environment, further swelling and bursting out of the endosome, thereby releasing the siRNA in the cytosol. Silencing of green fluorescent protein (GFP) was induced in MDA-MB-231/GFP cells by employing these nanoparticles (Fig. 10C), implying that these nanoparticles have the potential to serve as delivery vectors for multiple drugs and gene delivery. Recently, magnetic thermo-responsive nanocarriers (magnetic nanobeads coated with thermo-responsive polymers) were developed for controlled release of the drug molecules using combined thermal and magnetic activation [76]. This kind of nanocarriers is a promising candidate for localized drug delivery at specific tumor sites.

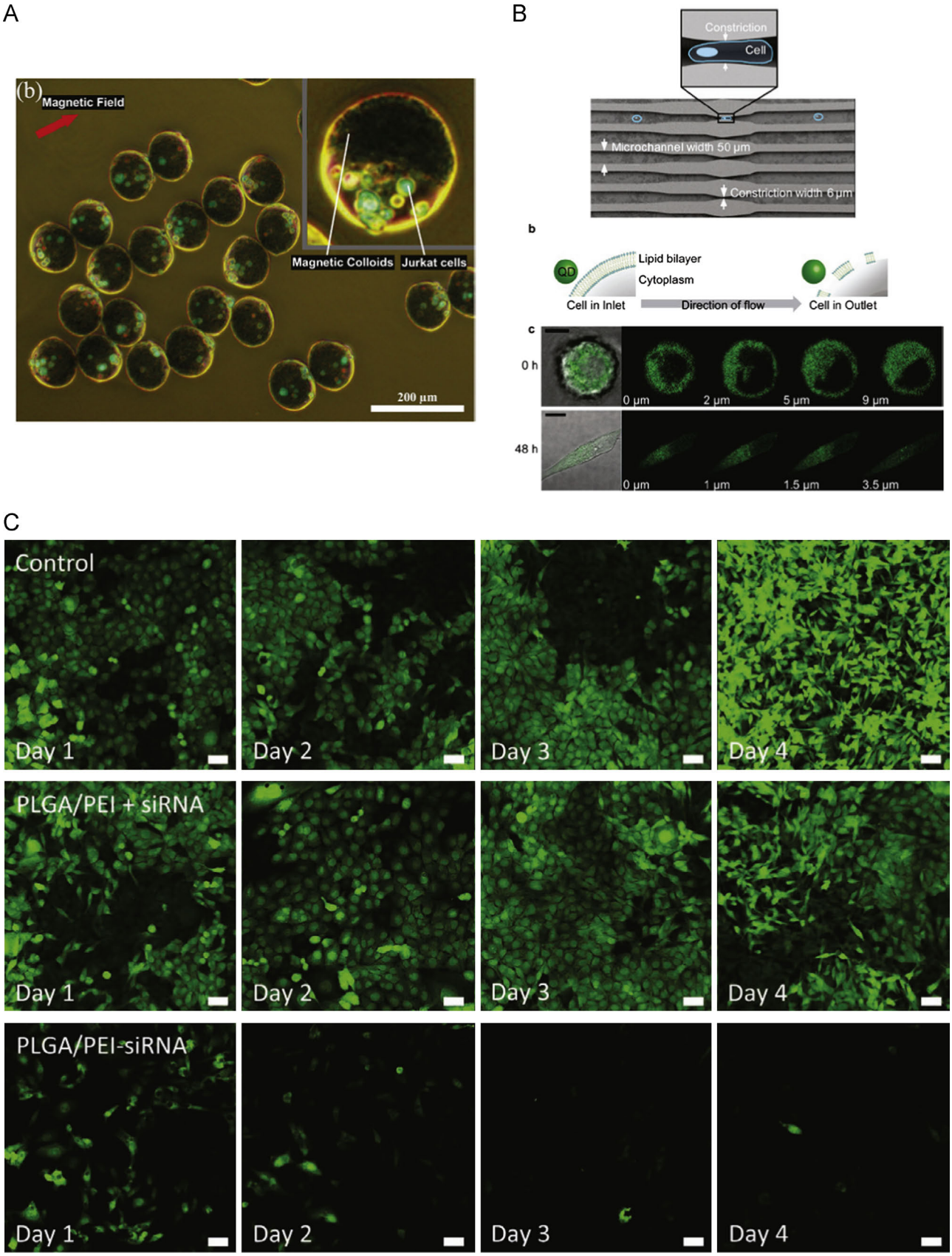

Fig. 10. Applications of MPs in cell encapsulation, imaging and therapy. (A) Magnetized Janus particles carrying living Jurkat cells in another hemisphere under an external magnetic field (reproduced with permission from Ref. [28]). (B) Schematic of the microfluidic device for delivering QDs into the cytoplasm of live cells, hypothesized method of entry for nanoparticles, and overlay of transmission and confocal fluorescence images, followed by *z*-section confocal fluorescence images of treated cells delivered with QDs (reproduced with permission from Ref. [71]). (C) *In vitro* incubation experiments of MDA-MB-231/GFP breast cancer cells with no particles or siRNA treatment (first row), with pure particles (PLGA/PEI) and soluble siRNA (not loaded in the particles, second row) and with siRNA-loaded particles (third row), respectively (reproduced with permission from Ref. [74]). Scale bars are 10 μm in (B), 50 μm in (C).

4. Challenges and outlook

In summary, MPs prepared in microfluidic systems have a host of advantages, such as precisely controlled morphology and size, fine structures, homogeneity, as well as their multiple functions in analytical applications. Nevertheless, the fabrication of MPs based on microfluidic systems is still in its infancy. Preparation of particles in nanoscale and with versatility remains highly challenging, which seriously blocks the particles from being employed in nanoscale applications. Despite the fact that some enlightened methods have been proved to be capable of generating multifunctional nanoparticles, accurately regulating the architectures and properties of the particles is still a hard nut to crack. It is undoubtedly extremely desired to develop brand new strategies for preparing MPs in microfluidic systems. Currently, materials available for MP preparation in microfluidic chips are rather limited. Apart from polymers, other materials, such as metals or carbon materials which present superior performances in catalysis and sensing, should come into notice. There is an increasing trend towards applications of MPs in biomedicine. Development of bionic intelligent MPs, such as self-powered MPs in physiological environment, will be of great significance in life science. In brief, fabrications and applications of MPs in microfluidic systems will hold great promise in not only analytical chemistry but also life science and biomedicine.

Acknowledgments

Financial support from the Natural Science Foundation of China (21375012 and 21305010), and the Fundamental Research Funds for the Central Universities (N110805001 and N110705002) is gratefully acknowledged.

References

[1] A.S. de Dios, M.E. Díaz-García, Anal. Chim. Acta 666 (2010) 1–22.
[2] S.T. Selvan, T.T.Y. Tan, D.K. Yi, N.R. Jana, Langmuir 26 (2010) 11631–11641.
[3] J. Du, R.K. O'Reilly, Chem. Soc. Rev. 40 (2011) 2402–2416.
[4] S. Yang, F. Guo, B. Kiraly, X. Mao, M. Lu, K.W. Leong, T.J. Huang, Lab Chip 12 (2012) 2097–2102.
[5] S. Marre, K.F. Jensen, Chem. Soc. Rev. 39 (2010) 1183–1202.
[6] D. Dendukuri, P.S. Doyle, Adv. Mater. 21 (2009) 4071–4086.
[7] J. Hu, S. Zhou, Y. Sun, X. Fang, L. Wu, Chem. Soc. Rev. 41 (2012) 4356–4378.
[8] T. Nisisako, T. Torii, T. Takahashi, Y. Takizawa, Adv. Mater. 18 (2006) 1152–1156.
[9] R.F. Shepherd, J.C. Conrad, S.K. Rhodes, D.R. Link, M. Marquez, D.A. Weitz, J.A. Lewis, Langmuir 22 (2006) 8618–8622.
[10] Z.H. Nie, W. Li, M. Seo, S.Q. Xu, E. Kumacheva, J. Am. Chem. Soc. 128 (2006) 9408–9412.
[11] L.B. Zhao, L. Pan, K. Zhang, S.S. Guo, W. Liu, Y. Wang, Y. Chen, X.Z. Zhao, H.L. W. Chan, Lab Chip 9 (2009) 2981–2986.
[12] C.H. Chen, A.R. Abate, D. Lee, E.M. Terentjev, D.A. Weitz, Adv. Mater. 21 (2009) 3201–3204.
[13] C.H. Chen, R.K. Shah, A.R. Abate, D.A. Weitz, Langmuir 25 (2009) 4320–4323.
[14] C. Cramer, P. Fischer, E.J. Windhab, Chem. Eng. Sci. 59 (2004) 3045–3058.
[15] W.J. Duncanson, T. Lin, A.R. Abate, S. Seiffert, R.K. Shah, D.A. Weitz, Lab Chip 12 (2012) 2135–2145.
[16] S.H. Kim, S.J. Jeon, W.C. Jeong, H.S. Park, S.M. Yang, Adv. Mater. 20 (2008) 4129–4134.
[17] Z. Yu, C.F. Wang, L. Ling, L. Chen, S. Chen, Angew. Chem. Int. Ed. 51 (2012) 2375–2378.
[18] S.N. Yin, C.F. Wang, Z.Y. Yu, J. Wang, S.S. Liu, S. Chen, Adv. Mater. 23 (2011) 2915–2919.
[19] R.K. Shah, J.W. Kim, D.A. Weitz, Adv. Mater. 21 (2009) 1949–1953.
[20] S.H. Kim, A. Abbaspourrad, D.A. Weitz, J. Am. Chem. Soc. 133 (2011) 5516–5524.
[21] Y. Zhao, H.C. Shum, H. Chen, L.L.A. Adams, Z. Gu, D.A. Weitz, J. Am. Chem. Soc. 133 (2011) 8790–8793.
[22] J. Wang, Y. Hu, R. Deng, W. Xu, S. Liu, R. Liang, Z. Nie, J. Zhu, Lab Chip 12 (2012) 2795–2798.
[23] K.H. Roh, D.C. Martin, J. Lahann, Nat. Mater. 4 (2005) 759–763.
[24] K.H. Roh, D.C. Martin, J. Lahann, J. Am. Chem. Soc. 128 (2006) 6796–6797.
[25] A. Kazemi, J. Lahann, Small 4 (2008) 1756–1762.
[26] S. Bhaskar, J. Lahann, J. Am. Chem. Soc. 131 (2009) 6650–6651.
[27] S. Bhaskar, J. Hitt, S.W.L. Chang, J. Lahann, Angew. Chem. Int. Ed. 48 (2009) 4589–4593.
[28] K. Maeda, H. Onoe, M. Takinoue, S. Takeuchi, Adv. Mater. 24 (2012) 1340–1346.
[29] J. Lee, J. Kim, Chem. Mater. 24 (2012) 2817–2822.
[30] D. Dendukuri, D.C. Pregibon, J. Collins, T.A. Hatton, P.S. Doyle, Nat. Mater. 5 (2006) 365–369.
[31] D.C. Pregibon, M. Toner, P.S. Doyle, Science 315 (2007) 1393–1396.
[32] D.C. Appleyard, S.C. Chapin, R.L. Srinivas, P.S. Doyle, Nat. Protoc. 6 (2011) 1761–1774.
[33] D. Dendukuri, T.A. Hatton, P.S. Doyle, Langmuir 23 (2007) 4669–4674.
[34] W.S. Tan, C.L. Lewis, N.E. Horelik, D.C. Pregibon, P.S. Doyle, H.M. Yi, Langmuir 24 (2008) 12483–12488.
[35] J.H. Jang, D. Dendukuri, T.A. Hatton, E.L. Thomas, P.S. Doyle, Angew. Chem. Int. Ed. 46 (2007) 9027–9031.
[36] K.W. Bong, D.C. Pregibon, P.S. Doyle, Lab Chip 9 (2009) 863–866.
[37] K.W. Bong, K.T. Bong, D.C. Pregibon, P.S. Doyle, Angew. Chem. Int. Ed. 49 (2010) 87–90.
[38] D. Dendukuri, S.S. Gu, D.C. Pregibon, T.A. Hatton, P.S. Doyle, Lab Chip 7 (2007) 818–828.
[39] D.K. Hwang, J. Oakey, M. Toner, J.A. Arthur, K.S. Anseth, S. Lee, A. Zeiger, K.J. Van Vliet, P.S. Doyle, J. Am. Chem. Soc. 131 (2009) 4499–4504.
[40] H.Z. An, M.E. Helgeson, P.S. Doyle, Adv. Mater. 24 (2012) 3838–3844.
[41] X. Zhao, Y. Cao, F. Ito, H.H. Chen, K. Nagai, Y.H. Zhao, Z.Z. Gu, Angew. Chem. Int. Ed. 45 (2006) 6835–6838.
[42] C. Sun, X.W. Zhao, Y.J. Zhao, R. Zhu, Z.Z. Gu, Small 4 (2008) 592–596.
[43] Y.J. Zhao, X.W. Zhao, C. Sun, J. Li, R. Zhu, Z.Z. Gu, Anal. Chem. 80 (2008) 1598–1605.
[44] H. Lee, J. Kim, H. Kim, J. Kim, S. Kwon, Nat. Mater. 9 (2010) 745–749.
[45] R. Karnik, F. Gu, P. Basto, C. Cannizzaro, L. Dean, W. Kyei-Manu, R. Langer, O.C. Farokhzad, Nano Lett. 8 (2008) 2906–2912.
[46] H. Xie, Z.G. She, S. Wang, G. Sharma, J.W. Smith, Langmuir 28 (2012) 4459–4463.
[47] S. Duraiswamy, S.A. Khan, Nano Lett. 10 (2010) 3757–3763.
[48] K. Kumar, A.M. Nightingale, S.H. Krishnadasan, N. Kamaly, M. Wylenzinska-Arridge, K. Zeissler, W.R. Branford, E. Ware, A.J. deMello, J.C. deMello, J. Mater. Chem. 22 (2012) 4704–4708.
[49] S. Birtwell, H. Morgan, Integr. Biol. 1 (2009) 345–362.
[50] D.C. Appleyard, S.C. Chapin, P.S. Doyle, Anal. Chem. 83 (2011) 193–199.
[51] R.L. Srinivas, S.C. Chapin, P.S. Doyle, Anal. Chem. 83 (2011) 9138–9145.
[52] Y.J. Zhao, X.W. Zhao, J. Hu, J. Li, W.Y. Xu, Z.Z. Gu, Angew. Chem. Int. Ed. 48 (2009) 7350–7352.
[53] D.C. Pregibon, P.S. Doyle, Anal. Chem. 81 (2009) 4873–4881.
[54] K.W. Bong, S.C. Chapin, P.S. Doyle, Langmuir 26 (2010) 8008–8014.
[55] S.C. Chapin, D.C. Appleyard, D.C. Pregibon, P.S. Doyle, Angew. Chem. Int. Ed. 50 (2011) 2289–2293.
[56] S.C. Chapin, P.S. Doyle, Anal. Chem. 83 (2011) 7179–7185.
[57] N.W. Choi, J. Kim, S.C. Chapin, T. Duong, E. Donohue, P. Pandey, W. Broom, W.A. Hill, P.S. Doyle, Anal. Chem. 84 (2012) 9370–9378.
[58] Y. Zhao, X. Zhao, B. Tang, W. Xu, J. Li, J. Hu, Z. Gu, Adv. Funct. Mater. 20 (2010) 976–982.
[59] H. Zhang, A.J. DeConinck, S.C. Slimmer, P.S. Doyle, J.A. Lewis, R.G. Nuzzo, Chem. Eur. J 17 (2011) 2867–2873.
[60] Y. Zhao, X. Zhao, J. Hu, M. Xu, W. Zhao, L. Sun, C. Zhu, H. Xu, Z. Gu, Adv. Mater. 21 (2009) 569–572.
[61] E. Chung, R. Gao, J. Ko, N. Choi, D.W. Lim, E.K. Lee, S.I. Chang, J. Choo, Lab Chip 13 (2013) 260–266.
[62] J.M. Köhler, A. März, J. Popp, A. Knauer, I. Kraus, J. Faerber, C. Serra, Anal. Chem. 85 (2013) 313–318.
[63] X. Yu, H.S. Xia, Z.D. Sun, Y. Lin, K. Wang, J. Yu, H. Tang, D.W. Pang, Z.L. Zhang, Biosens. Bioelectron. 41 (2013) 129–136.
[64] Y. Daghighi, D. Li, Lab Chip 11 (2011) 2929–2940.
[65] C. Hou, Q. Zhang, H. Wang, Y. Li, J. Mater. Chem. 21 (2011) 10512–10517.
[66] N.S. Satarkar, W. Zhang, R.E. Eitel, J.Z. Hilt, Lab Chip 9 (2009) 1773–1779.
[67] L. Baraban, D. Makarov, R. Streubel, I. Monch, D. Grimm, S. Sanchez, O.G. Schmidt, ACS Nano 6 (2012) 3383–3389.
[68] S.H. Kim, J.Y. Sim, J.M. Lim, S.M. Yang, Angew. Chem. Int. Ed. 49 (2010) 3786–3790.
[69] S. Sanchez, A.A. Solovev, S.M. Harazim, O.G. Schmidt, J. Am. Chem. Soc. 133 (2011) 701–703.
[70] M. Yoshida, K.H. Roh, S. Mandal, S. Bhaskar, D. Lim, H. Nandivada, X. Deng, J. Lahann, Adv. Mater. 21 (2009) 4920–4925.
[71] J. Lee, A. Sharei, W.Y. Sim, A. Adamo, R. Langer, K.F. Jensen, M.G. Bawendi, Nano Lett. 12 (2012) 6322–6327.
[72] L. Cheng, X. Zhang, Z. Zhang, H. Chen, S. Zhang, J. Kong, Talanta 115 (2013) 823–829.
[73] J. Ai, Y. Xu, B. Lou, D. Li, E. Wang, Talanta 118 (2014) 54–60.
[74] A.C. Misra, S. Bhaskar, N. Clay, J. Lahann, Adv. Mater. 24 (2012) 3850–3856.
[75] C.H. Yang, K.S. Huang, Y.S. Lin, K. Lu, C.C. Tzeng, E.C. Wang, C.H. Lin, W.Y. Hsu, J.Y. Chang, Lab Chip 9 (2009) 961–965.
[76] M.P. Leal, A. Torti, A. Riedinger, R. La Fleur, D. Petti, R. Cingolani, R. Bertacco, T. Pellegrino, ACS Nano 6 (2012) 10535–10545.
[77] A. Sharei, J. Zoldan, A. Adamo, W.Y. Sim, N. Cho, E. Jackson, S. Mao, S. Schneider, M.J. Han, A. Lytton-Jean, P.A. Basto, S. Jhunjhunwala, J. Lee, D.A. Heller, J.W. Kang, G.C. Hartoularos, K.S. Kim, D.G. Anderson, R. Langer, K.F. Jensen, Proc. Natl. Acad. Sci. USA 110 (2013) 2082–2087.